General Analytical Description of Spin-Diffusion for a Three-Domain Morphology. Application to Melt-Spun Nylon 6 Fibers

A. Buda, D. E. Demco, M. Bertmer, and B. Blümich*

Institut für Technische Chemie und Makromolekulare Chemie, Rheinisch-Westfälische Technische Hochschule, Worringer Weg 1, D-52056 Aachen, Germany

V. M. Litvinov

DSM Research, P.O. Box 18, 6160 MD Geleen, The Netherlands

J. P. Penning

DSM Fiber Intermediates, P.O. Box 18, 6160 MD Geleen, The Netherlands

Received: July 22, 2002; In Final Form: December 16, 2003

The NMR spin-diffusion process taking place in a morphology represented by three different domains with arbitrary sizes and diffusivities is investigated. General analytical solutions valid for the full range of spin-diffusion times were obtained for a one-dimensional lamellar morphology. The accuracy of these solutions has been tested by predicting the domain sizes for a poly(styrene-*b*-methyphenylsiloxane) diblock copolymer and semicrystalline poly(ethylene oxide) and comparing them with previously reported data. The effects of large changes in the size of the interface domain and the spin-diffusion coefficients of this domain on the spin-diffusion decay and build-up curves can be analyzed by numerical simulations. General analytical solutions of the spin-diffusion equations were used for investigating the complex morphology of high-speed melt-spun nylon 6 fibers. The NMR mobile amorphous, NMR less-mobile amorphous, and crystalline phases of nylon 6 fibers hydrated with D_2O were detected and quantified using ^1H spectra and spin−lattice relaxation rates. Proton spin-diffusion experiments were performed on nylon 6 fibers using a dipolar filter based on magic- and polarization-echoes for the mobile amorphous phase. The results of this experiment can be interpreted by considering that the ^1H magnetization front which emanates from the mobile amorphous phase explores crystalline/less-mobile amorphous aggregates. The domain sizes of the mobile amorphous phase, the interface, and aggregates can be estimated using analytical solutions of the spin-diffusion equations and correlated with the spinning speed and the draw ratio of the nylon 6 fibers.

I. Introduction

A broad class of materials such as polymers, composite materials, or biomaterials shows microheterogeneities in both structural and associated dynamical properties. These distributed microstructures can be probed by a variety of methods such as transmission electron microscopy (TEM), field ion and atomic force microscopy (AFM), small-angle X-ray scattering (SAXS), and neutron scattering (SANS). Solid-state NMR microscopy and NMR imaging have opened up new possibilities in this area as a direct result of the high spectral selectivity and the space encoding capability by magnetic field gradients.[1−4]

The NMR spin-diffusion or magnetization transfer experiment taking place on a mesoscopic scale is mediated by the dipolar couplings and provides information on different aspects of structural heterogeneities in a broad range of spatial dimensions from 0.1 nm to about 200 nm.[1,5−11] Despite the impressive efforts to analyze quantitatively the spin-diffusion process, several fundamental problems remain to be solved.[12−14] It is mainly the one-dimensional or lamellar model, with a two- or three-phase morphology, that has been considered earlier in analytical[5,11−14] and numerical solutions[15−18] of the spin-diffusion equations. In many cases the analytical solutions which provide more physical insight into the spin-diffusion process were used in the short-time regime to obtain information about the domain sizes. For the spin-diffusion process taking place in two domains with lamellar, cylindrical, and spherical morphologies, analytical solutions for the evolution of magnetization in the domains were proposed.[11] An average spin-diffusion coefficient was assumed in order to simplify the complex relationships and to investigate the possibility of using spin-diffusion experiments to differentiate between different morphologies. This simplified description proved adequate for performing spatially resolved spin-diffusion measurements on solid polymers.[19] Later, general analytical solutions of the diffusion equations were derived for a two-domain lamellar morphology characterized by different spin-diffusion coefficients.[20]

The spin-diffusion method can be applied to characterize the polymer phase changes induced in the process of fiber fabrication. In ultradrawn, ultrahigh molecular weight polyethylene (PE) fibers, ^1H spin-diffusion yields amorphous domain sizes

* To whom correspondence should be addressed. Electronic mail: bluemich@mc.rwth-aachen.de.

10.1021/jp021684v CCC: $25.00
Published on Web 05/13/2003

of 10 ± 5 nm, and crystalline regions of 100 ± 50 nm diameters were estimated.[21] Simulations based on a one-dimensional lamellar morphology were performed to estimate the smallest size of the domains. Nevertheless, it is claimed that a dimensionality of two is a more reasonable assumption to model the spin-diffusion process. A second, highly mobile, amorphous phase making up a small amount of the sample was detected and seems to be a universal feature of ultradrawn PE fibers. The experiment shows that very little spin-diffusion from the highly mobile phase to the other two phases was observed even after 200 ms of magnetization transfer.[21]

A series of fibers of poly(ethylene terephthalate) (PET) with different physical structures has also been investigated by ^{13}C solid-state NMR measurements.[22] Analysis of the line-shape changes during spin−lattice relaxation in the rotating frame $T_{1\rho}$(^{13}C) of the PET fibers showed that the NMR amorphous phase relaxes with two time constants. A three-domain model composed of crystalline, rigid amorphous, and mobile amorphous regions was proposed. From $T_{1\rho}(^1H)$ experiments it was concluded that both mobile and rigid amorphous regions have dimensions smaller than 5 nm.

Polyamides (PA) are well-known as high-performance engineering materials. Nylon 6 (PA6) is one of the most important synthetic fiber-forming materials used for high-speed melt spinning.[23] High-speed melt spinning is of great scientific interest and technical importance. Therefore, it is necessary to understand the relationship between the spinning speed and the fiber properties on the basis of the microscopic structure and molecular motion.

The segmental dynamics of nylon 66 were investigated by deuterium NMR spin−lattice relaxation and line-shape simulations. They revealed the existence of "free" and "constrained" amorphous populations.[24,25] This result is confirmed by studies by X-ray diffraction which indicate that there are three different phases in nylon 6 fibers: crystalline, unorientated amorphous located in the lamellar stack, and orientated amorphous located between the fibrils.[26,27] Furthermore, the existence of a mobile amorphous phase aditionally to the crystalline and rigid amorphous phases in nylon 6 fibers has been proved by measurements of the ^1H spin−lattice relaxation in the rotating frame ($T_{1\rho}$), and a processing-microstructure and chain motion relationship was established.[28,29] The fraction of each phase was estimated from the $T_{1\rho}$ magnetization decay. It was shown that it is dependent on the processing spinning speed. The NMR mobile amorphous phase represents a small fraction of a few percent compared to the crystalline and NMR rigid amorphous phases. It can be inferred from NMR spin−lattice relaxation measurements that the rigid amorphous regions, rather than the mobile amorphous ones, transform into the crystalline regions during high-speed spinning of nylon 6 fibers. In addition to NMR spectroscopy and relaxometry, magnetic resonance imaging has been also used to investigate the fracture behavior of two different types of extruded polyamide 6/maleic anhydride grafted ethylene−propylene (EPM-*g*-MA) blends.[30]

Recently, an investigation of the changes in the crystallinity and morphology of some paramagnetic nylon-6 clay nanocomposites compared with the corresponding pure nylon-6 samples was made by ^1H spin-diffusion measurements.[10]

The main objectives of this work are as follows: (i) To obtain general analytical solutions for the spin-diffusion equations describing the process of longitudinal magnetization transfer in a one-dimensional morphology composed of three domains with arbitrary sizes and diffusivities. The spin-diffusion equations need to be solved taking into account proper initial and boundary conditions. The domain sizes obtained by using these analytical solutions have been tested using previously published spin-diffusion data on diblock copolymers and semicrystalline polymers. (ii) To use the general analytical description of the spin-diffusion experiment for investigating the morphology of high-speed melt-spun nylon 6 fibers hydrated with D_2O by applying a dipolar filter to select the ^1H longitudinal magnetization in the mobile amorphous regions. The changes in the detected domain sizes are correlated with the spinning speed and the draw ratio of the nylon 6 fibers.

TABLE 1: Processing Parameters of Nylon 6 Fibers

winding speed (m/min)	draw ratio	polymer	M_n (g/mol)	tenacity (cN/dtex)	elongation at break (%)
500		GL2000	21 400	1.20	358
500	4.5	GL2000	21 400	6.49	20.4
5000		GL1030	16 400	4.39	62.5

II. Experiment

A. Samples. Nylon 6 multifilament yarns used in this study were obtained by melt-spinning at DSM (Geleen, The Netherlands). Two different spinning speeds were applied: 500 and 5000 m/min. The fiber spun at 500 m/min was obtained from a polymer with $M_n = 21\,400$ g/mol (Nylon 6 technical grade). The fiber spun at 5000 m/min was obtained from a polymer with $M_n = 16\,400$ g/mol (Nylon 6 textile grade). The diameters of the individual filaments in the as-spun yarns obtained at 500 and 5000 m/min are 50 and 13 μm, respectively. An additional sample was obtained by drawing the fiber spun at 500 m/min to a draw ratio of DR = 4.5. After drawing, the individual filaments have a diameter of about 25 μm. The characteristics of the nylon 6 fibers are summarized in Table 1.

To avoid complications in the interpretation of NMR spin-diffusion data introduced by the presence of the absorbed water, the nylon 6 fibers were saturated with D_2O by putting them in contact with the D_2O liquid. Equilibrium was reached after 1 week when no weight change was recorded on successive days. For nylon 6 fibers at room temperature for a relative humidity of the surrounding air of 100% and 40%, the fiber mass is increasing by about 10% and 2%, respectively. The hydration water is present only in the amorphous phase of the nylon 6 fibers,[31,32] and because the amount of water uptake is moderate,[33] no drastic changes in the domain sizes are expected.

B. NMR Experiments. Proton solid-state NMR spectra and spin-diffusion data were measured using a Bruker DSX-500 spectrometer operating at 500.45 MHz for ^1H. The data were collected for static samples at room temperature. The length of the $\pi/2$ pulse was about 5.5 μs, and the dwell time was set to 2.5 μs. The dead time of the spectrometer is 2.5 μs. The recycle delay was 7.5 s for all measurements. The NMR experiments with the nylon 6 fibers immersed in D_2O and those hydrated with D_2O essentially showed the same ^1H spectra. The ^1H spectra can be decomposed in three components (see below) using the Bruker WinFit program.

Proton longitudinal magnetization relaxation (T_1) measurements for nonrotating samples were performed at room temperature using the inversion recovery method. To avoid magnetization transfer from the mobile amorphous phase to the rigid amorphous and crystalline phases, additional measurements

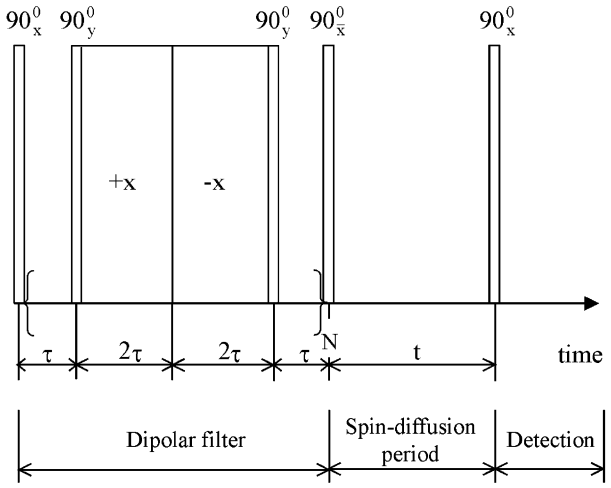

Figure 1. Pulse sequence used for the spin-diffusion experiment. A dipolar filter based on magic- and polarization-echoes (MAPE filter) was used.[11] The number of applied magic sandwiches and the spin-diffusion time are denoted by N and t, respectively.

under magic-angle sample spinning (MAS) were made at a rotor frequency of $\nu_R = 5$ kHz, this time using the saturation recovery method. Typically 35−40 increment times were used, and the total integral intensities of the NMR absorption spectra were fitted with a sum of two exponentials by a least-squares procedure. The fast decaying component was attributed to the mobile amorphous phase, and the other one, to the rigid amorphous and crystalline phases. These measurements do not allow us to separate the longitudinal magnetization relaxations of the last two phases. Nevertheless, longitudinal relaxation in the rotating reference frame ($T_{1\rho}$) is able to reveal the existence of three different NMR motional phases.[28,29]

The spin-diffusion experiment follows the general scheme "z-magnetization filter−spin-diffusion period−detection" as shown in Figure 1.[1] As a dipolar filter, the MAPE sequence (cf. Figure 1) was used for all the measurements.[11] The value of the parameter τ used for the dipolar filter in nylon 6 samples was $\tau = 110$ μs. For all the measurements the dipolar filter selects the z-magnetization in the mobile amorphous domains. The spin-diffusion data were corrected for the T_1 relaxation using the procedure described in ref 1. The integral intensity of the signal from the mobile amorphous phase was multiplyed by $\exp(t/T_1)$ with the corresponding T_1 value. Because the amount of the mobile amorphous phase is small and the spin-diffusion process slow, we have been able to detect only a slight increase of the NMR signal corresponding to the rigid amorphous and crystalline phases even at very long spin-diffusion times.

III. Theory

A. General Analytical Solutions of Spin-Diffusion Equations. We consider that the spin-diffusion process takes place in a lamellar morphology (Figure 2). The nuclear magnetization transfer occurs from a source A into a finite sink B via an interface I. The process is one-dimensional along the x direction corresponding to the smallest distances. Actually, the interface can be, in principle, a domain with a size comparable to the sizes of domains A and B. In each region the spin-diffusion process is supposed to be governed by the macroscopic

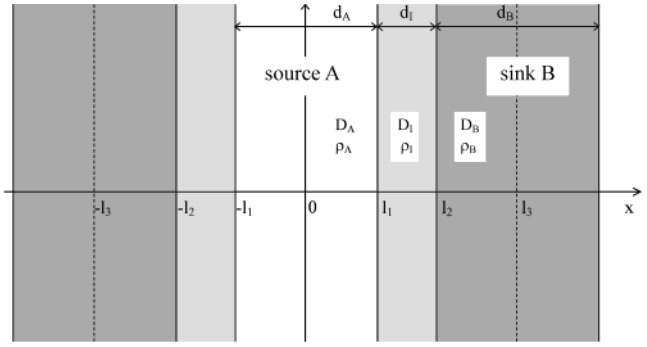

Figure 2. Schematic representation of the finite-source/interface/finite-sink system with lamellar morphology. The spin-diffusion is considered to be one-dimensional along the x-axis across the domain boundaries. The source, interface, and sink domains have the linear dimensions d_A, d_I, and d_B, respectively, and they have been supposed to be much smaller than the dimension perpendicular to the diffusion direction. The spin-diffusion diffusivities are D_A, D_I, and D_B, and the spin densities are denoted by ρ_A, ρ_I, and ρ_B.

law of Fick, that is,

$$\frac{\partial^2 m_A(x,t)}{\partial x^2} - \frac{1}{D_A}\frac{\partial m_A(x,t)}{\partial t} = 0$$

$$\frac{\partial^2 m_I(x,t)}{\partial x^2} - \frac{1}{D_I}\frac{\partial m_I(x,t)}{\partial t} = 0$$

$$\frac{\partial^2 m_B(x,t)}{\partial x^2} - \frac{1}{D_B}\frac{\partial m_B(x,t)}{\partial t} = 0 \qquad (1)$$

where m_A, m_B, and m_I are the space (x) and time (t) dependent concentrations of the nuclear z-magnetization in the corresponding domains. D_A, D_B, and D_I are the spin-diffusion coefficients in the domains A, B, and I, respectively. It is assumed that they are independent of space and the amount of magnetization.

The linear sizes of the domains A, B, and I along the direction of the polarization transfer are denoted by d_A, d_B, and d_I, respectively. Because of the symmetry of the morphology, the calculations will be made only for positive x coordinates, so that for region A, we have $0 \le x < l_1$, for region I, $l_1 \le x < l_2$, and, for region B, $l_2 \le x < l_3$ (cf. Figure 2).

At zero spin-diffusion time the whole magnetization is supposed to be concentrated in domain A (source); that is,

$$m_A(t=0) = m_0 \qquad (2)$$

$$m_I(t=0) = 0 \quad \text{and} \quad m_B(t=0) = 0 \qquad (3)$$

Then the magnetization flows from A to B via domain I respecting the boundary conditions. The first boundary conditions are related to the continuity of the z-magnetization (or nuclear polarization oriented parallel to the direction of the static magnetic field) concentration at the domain boundaries. They can be written as

$$m_A(l_1,t) = m_I(l_1,t) \qquad (4)$$

$$m_I(l_2,t) = m_B(l_2,t) \qquad (5)$$

The second boundary conditions require that the z-magnetization fluxes have to be equal at the domain interfaces; that is,

$$\rho_A D_A \frac{\partial m_A(l_1,t)}{\partial x} = \rho_I D_I \frac{\partial m_I(l_1,t)}{\partial x} \quad (6)$$

$$\rho_I D_I \frac{\partial m_I(l_2,t)}{\partial x} = \rho_B D_B \frac{\partial m_B(l_2,t)}{\partial x} \quad (7)$$

where ρ_A, ρ_B, and ρ_I are the number densities of spins in the A, B, and I domains, respectively.

It is also evident that

$$\left.\frac{\partial m_A(x,t)}{\partial x}\right|_{x=0} = 0 \quad \text{and} \quad \left.\frac{\partial m_B(x,t)}{\partial x}\right|_{x=l_3} = 0 \quad (8)$$

The solutions of the above differential equations with the initial and the boundary conditions can be obtained using the Laplace transformation. They are presented in the Appendix.[34,35]

We are finally interested in the spin-diffusion time dependence of the NMR signal intensity (NMR observable) of each domain, which is nothing else other than the integral of the concentration of the *z*-magnetization over the relevant dimension of each domain. Using the time and space dependent magnetization concentrations m_A, m_I, and m_B given in the Appendix (see eqs A15−A17), we finally get

$$I_A(t) = 2\int_0^{l_1} \rho_A m_A \, dx = \frac{2m_0 {\rho_A}^2 {l_1}^2}{\rho_A l_1 + \rho_I(l_2 - l_1) + \rho_B(l_3 - l_2)} - \sum_{m=1}^{\infty} \frac{8m_0\rho_I\sqrt{D_I}\rho_A e^{-D_A\beta_m^2 t}\sin(\beta_m l_1)}{{\beta_m}^2 F}\left\{(\rho_I\sqrt{D_I} + \rho_B\sqrt{D_B})\sin\left[\beta_m\left((l_3 - l_2)\sqrt{\frac{D_A}{D_B}} + (l_2 - l_1)\sqrt{\frac{D_A}{D_I}}\right)\right] + (\rho_I\sqrt{D_I} - \rho_B\sqrt{D_B})\sin\left[\beta_m\left(-(l_3 - l_2)\sqrt{\frac{D_A}{D_B}} + (l_2 - l_1)\sqrt{\frac{D_A}{D_I}}\right)\right]\right\} \quad (9)$$

$$I_I(t) = \int_{l_1}^{l_2} \rho_I m_I \, dx = \frac{m_0\rho_A l_1 \rho_I (l_2 - l_1)}{\rho_A l_1 + \rho_I(l_2 - l_1) + \rho_B(l_3 - l_2)} - \sum_{m=1}^{\infty} \frac{2m_0\rho_I\sqrt{D_I}e^{-D_A\beta_m^2 t}}{\sqrt{D_A}{\beta_m}^2 F}\left\{(\rho_I\sqrt{D_I} + \rho_B\sqrt{D_B})\sin\left[\beta_m\left((l_3 - l_2)\sqrt{\frac{D_A}{D_B}} + (l_2 - l_1)\sqrt{\frac{D_A}{D_I}}\right)\right] + (\rho_I\sqrt{D_I} - \rho_B\sqrt{D_B})\sin\left[\beta_m\left(-d(l_3 - l_2)\sqrt{\frac{D_A}{D_B}} + (l_2 - l_1)\sqrt{\frac{D_A}{D_I}}\right)\right]\right\}\left\{(\rho_I\sqrt{D_I} + \rho_A\sqrt{D_A})\sin\left[\beta_m\left(l_1 + (l_2 - l_1)\sqrt{\frac{D_A}{D_I}}\right)\right] - (\rho_I\sqrt{D_I} - \rho_A\sqrt{D_A})\sin\left[\beta_m\left(l_1 - (l_2 - l_1)\sqrt{\frac{D_A}{D_I}}\right)\right] - 2\rho_A\sqrt{D_A}\sin(\beta_m l_1)\right\} \quad (10)$$

and

$$I_B(t) = 2\int_{l_2}^{l_3} \rho_B m_B \, dx = \frac{2m_0\rho_A l_1 \rho_B (l_3 - l_2)}{\rho_A l_1 + \rho_I(l_2 - l_1) + \rho_B(l_3 - l_2)} + \sum_{m=1}^{\infty} \frac{16m_0\rho_I\rho_B\sqrt{D_B D_I}\rho_A e^{-D_A\beta_m^2 t}\sin(\beta_m l_1)}{{\beta_m}^2 F}\sin\left[\beta_m\left((l_3 - l_2)\sqrt{\frac{D_A}{D_B}}\right)\right] \quad (11)$$

This solution of the spin-diffusion process in a lamellar morphology composed of three domains is valid for arbitrary values of domain sizes and spin-diffusion coefficients. The limiting case of a finite-source/infinite-sink can easily be obtained from eqs 9−11.

The first test of the validity of the spin-diffusion NMR observables given by eqs 9−11 is related to the law of conservation of *z*-magnetization in time, that is,

$$I_A(t) + 2I_I(t) + I_B(t) = I_A(0) = \rho_A d_A m_0 \quad (12)$$

Moreover, in the particular situation of a vanishing interface, the NMR observables $I_A(t)$ and $I_B(t)$ (cf. eqs 9 and 11) are identical to those given in ref 20.

In many polymer systems we have to consider an ensemble average over a distribution of sizes in each domain. The time evolution of the spin-diffusion observables does not critically depend on the form of the size distribution function[11] (and references therein) and can easily be incorporated in our general solutions (eqs 9−11). In the interpretation of the spin-diffusion data given below, we will neglect this domain size distribution.

The solutions for a two (2D)- and a three (3D)-dimensional problem can be derived as products of the 1D solutions if the phase structure can be expressed as a product of one-dimensional structures.[5] Nevertheless, it is evident that the exact solutions for the spin-diffusion equations for cylindrical or spherical morphologies are different from those taken from a lamellar morphology.[11,34,35] It is beyond the scope of this work to obtain general solutions for such complex morphologies.

B. Effect of the Interface Domain. The general description of spin-diffusion for a three-domain system with arbitrary sizes and diffusivities allows us to simulate the effect of the approximations used for the value of spin diffusivity D_I of the interface domain. The spin-diffusion decay and build-up curves are simulated in Figure 3a for different values of D_I fulfilling the condition $D_A \le D_I \le D_B$. It is evident that the spin-diffusion curves are not very sensitive to the values taken for D_I. Hence, the arithmetic average $D_I = (D_A + D_B)/2$ used in the previous studies is justified.

The effect of the interface domain size d_I is simulated in Figure 3b. If the range of the d_I values changes about 1 order of magnitude, a clear change in the shape of the spin-diffusion curves is observed. It is shown in Figure 3b that for intermediate values of the spin-diffusion time the build-up curves have a good linear behavior. An approximate evaluation of the interface size can be obtained from the intercept of the time axis and the tangent to the linear region of the spin-diffusion build-up curves.[11] This value is given by $\sqrt{t_0}$ (cf. Figure 3b). In Figure 4 the d_I values are shown versus $\sqrt{t_0}$ obtained from a set of spin-diffusion simulations. It is evident that a linear dependence $d_I \propto \sqrt{t_0}$ exists only for the interface sizes up to about 1 nm. For a morphology represented by three domains with d_I values of the same order of magnitude as that for the source or sink,

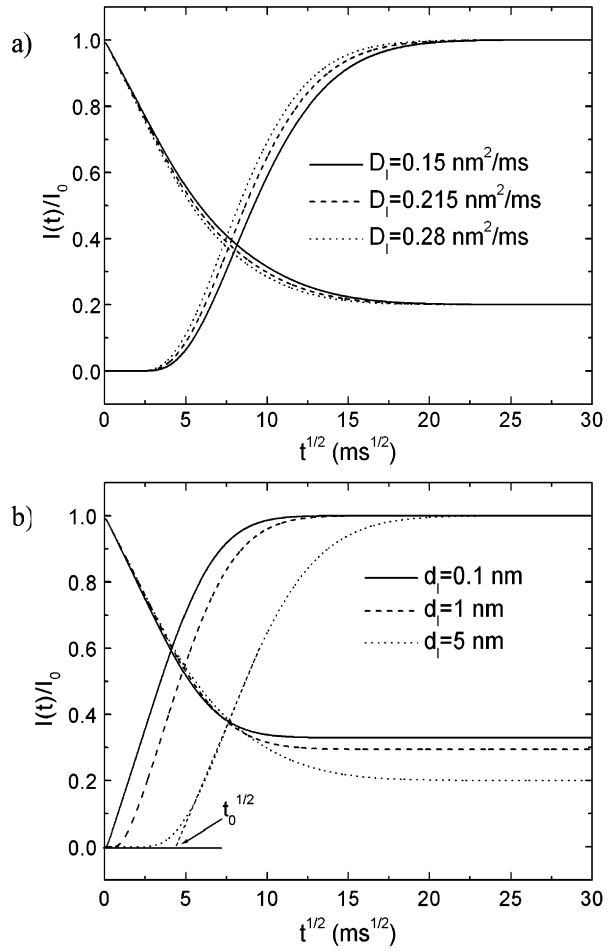

Figure 3. Effects of the spin-diffusion coefficient D_I (a) and the size d_I of the interface domain (b) on decay and build-up spin-diffusion curves simulated using eqs 9 and 11. For all the simulations the following parameters were used: $d_A = 5$ nm, $d_B = 10$ nm, $D_A = 0.15$ nm^2/ms, and $D_B = 0.28$ nm^2/ms. For the simulations shown in part a, the size of the interface domain was taken to be $d_I = 5$ nm, and in part b, the diffusion coefficient of the interface was $D_I = 0.215$ nm^2/ms. The intercept of the tangent to the linear region of the spin-diffusion build-up curve and the time axis is denoted by $t_0^{1/2}$.

the intercept $\sqrt{t_0}$ has a complex dependence on the interface domain size.

C. Tests for the Solutions of the Spin-Diffusion Equations. To check the accuracy of analytical solutions for spin-diffusion equations derived above, we shall apply them for the evaluation of the domain sizes in polymer systems with lamellar morphologies using data which have already been published in the literature.

The first case is represented by the sample C2 of a poly(styrene-*b*-methyphenylsiloxane) (PS-*b*-PMPS) diblock copolymer from ref 36. Its morphology is lamellar and had been determined by transmission electron microscopy. The previous study[36] also indicates the presence of an interface in this system which can be inferred from the sigmoidal shape of the spin-diffusion build-up curve at the beginning of the spin-diffusion process (see also Figure 3b).[1,5]

In Figure 5 the experimental data taken from ref 36 as well as the simulations based on our analytical solutions (cf. eq 11) are shown using the spin-diffusion coefficients and domain sizes given in refs 36 and 20 (see Table 2). The time dependent spin-diffusion curves simulated with the parameters from refs 36 and 20 are both in good agreement, but the experimental data

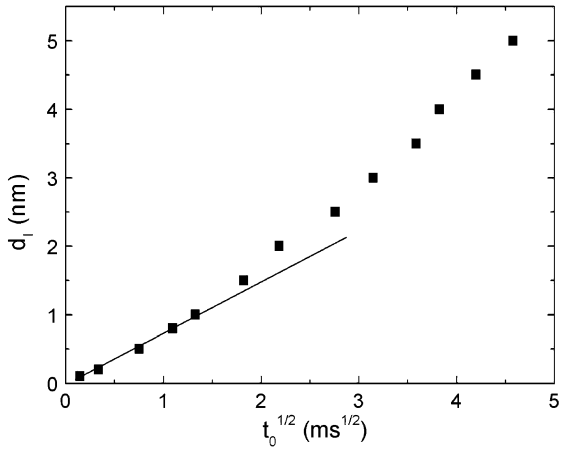

Figure 4. Interface size versus the intercept $t_0^{1/2}$ (see Figure 3b) obtained from a set of simulations based on eq 11 with $d_A = 5$ nm, $d_B = 10$ nm, and spin-diffusion coefficients $D_A = 0.15$ nm^2/ms, $D_B = 0.28$ nm^2/ms, and $D_I = 0.215$ nm^2/ms. The straight line shows that a linear dependence exists between d_I and $t_0^{1/2}$ for small values of the interface size.

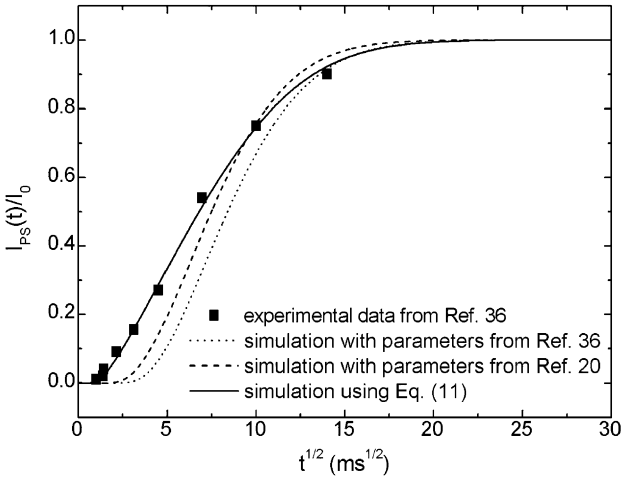

Figure 5. Experimental data for the ^{1}H spin-diffusion build-up curve of PS in a PS-*b*-PMPS diblock copolymer (sample C2 from ref 36). The integral intensity of the filtered spectrum is I_0. The solid line represents the fit of the experimental data using eq 11. The best fit parameters are given in Table 2. The simulations obtained using eq 11 with the diffusivities and domain sizes reported in ref 36 (dashed line) and ref 20 (dash−pointed line) are also shown. The spin-diffusion build-up curve and the experimental data were normalized to the quasi-equilibrium value.

TABLE 2: Spin-Diffusion Coefficients (*D*) and Domain Sizes (*d*) for a PS-*b*-PMPS Diblock Copolymer (First Rows)[36,20] and Values of the Diffusivities Used for the Simulation of the Spin-Diffusion Data Shown in Figure 5 and the Domain Sizes Obtained (Last Row)

D_{PMPS} (nm^2/ms)	$D_{interface}$ (nm^2/ms)	D_{PS} (nm^2/ms)	d_{PMPS} (nm)	$d_{interface}$ (nm)	d_{PS} (nm)
0.05[20,36]	0.3[20,36]	0.6[20,36]	5[36]	4[36]	9.5[36]
			5.5[20]	2.5[20]	12[20]
0.05	0.3	0.6	6.8[a]	1.3[a]	12.8[a]

[a] The uncertainties are less than 10%.

are not reproduced accurately. The build-up curve given by eq 11 is also shown in Figure 5, and the agreement with the experimental data is satisfactory for all values of the spin-diffusion times. The diffusion coefficients and the domain sizes which give the best fit with the experimental data are given in Table 2. They are close to the values reported previously.[36,20]

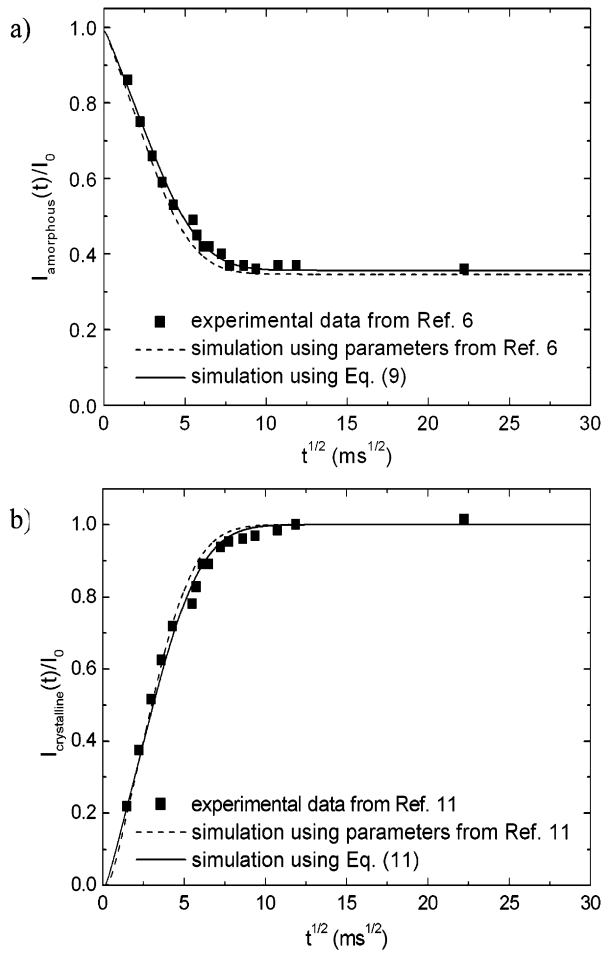

Figure 6. Time evolution for the ^1H spin-diffusion observables of amorphous (a) and crystalline (b) components of PEO from ref 11. The dashed lines show the curves obtained from eqs 9 and 11 with the parameters from ref 11. The solid lines represent the fit of the spin-diffusion data using eq 9 for part a and eq 11 for part b. The best fit parameters are presented in Table 3. The spin-diffusion build-up curve and the experimental data were normalized to the quasi-equilibrium value.

TABLE 3: Spin-Diffusion Coefficients (*D*) and Domain Sizes (*d*) for the PEO System (First Row)[11] and Values of the Diffusivities Used for Simulation of the Spin-Diffusion Data Shown in Figure 6 and the Domain Sizes Obtained (Last Row)

$D_{amorphous}$ (nm^2/ms)	$D_{interface}$ (nm^2/ms)	$D_{crystalline}$ (nm^2/ms)	$d_{amorphous}$ (nm)	$d_{interface}$ (nm)	$d_{crytalline}$ (nm)
0.15[11]	0.215[11]	0.28[11]	4.1[11]	0.32[11]	7.1[11]
0.15	0.215	0.28	4.6[a]	0.15[a]	8[a]

[a] The uncertainties are less than 10%.

Moreover, the long period of the lamellar morphology obtained from our data, that is, $d_{NMR} = d_{PMPS} + 2d_{interface} + d_{PS}$, is $d_{NMR} \approx 22.2 \pm 2$ nm and lies in the range of the values measured by SAXS, $d_{SAXS} \approx 19-25$ nm.[36]

The second case is given by high molecular weight poly(ethylene oxide) (PEO). It has crystalline and amorphous lamellar domains which have been investigated by spin-diffusion experiments.[11] The measured spin-diffusion decay and build-up curves for the amorphous and the crystalline regions from ref 11 are shown in Figure 6. Using eqs 9 and 11 and spin-diffusion coefficients as well as the domain sizes reported in ref 11 (see Table 3), the time evolutions of the NMR signals from amorphous and crystalline domains are shown in Figure 6 (dashed lines). The differences between the experimental data and the simulated spin-diffusion curves using our general solutions are due to the fact that, for estimating the domain sizes in ref 11, simplified solutions of the spin-diffusion equations were used, with an average spin-diffusion coefficient.[34] The best fits of the spin-diffusion data[11] using eqs 9 and 11 are given by solid lines (cf. Figure 6). The best fit parameters are listed in Table 3. The use of exact solutions for the spin-diffusion process in which each region is characterized by a different diffusivity in the case of semicrystalline PEO leads to larger domain sizes compared to the case of an average diffusivity.[11] This is due to the fact that the fronts of the *z*-magnetization in the crystalline domains which have the largest size will travel faster because the diffusivity of these domains is larger compared to the average of the diffusivities.

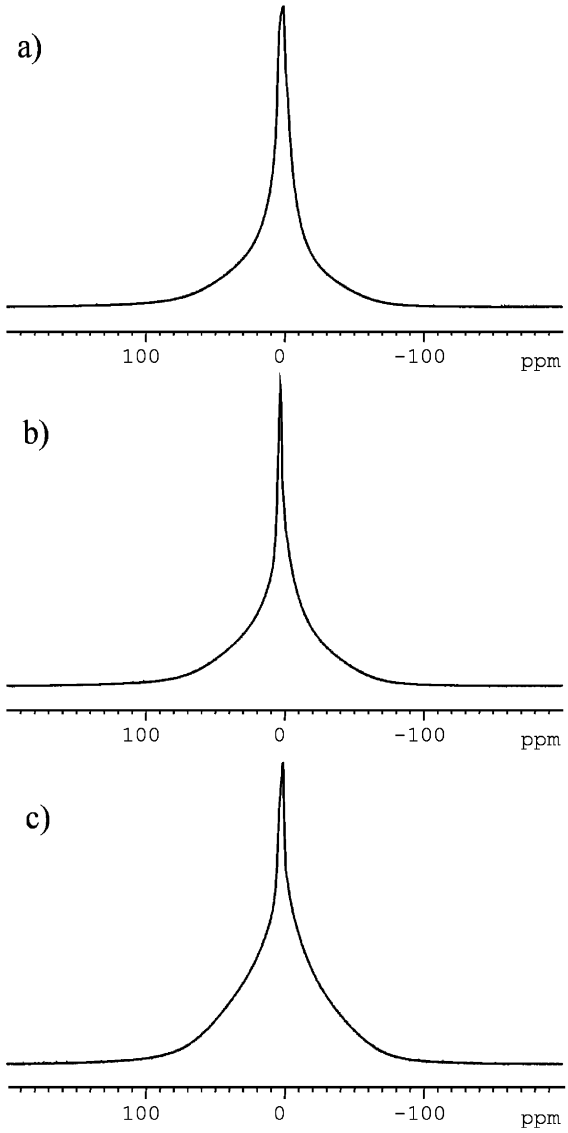

Figure 7. Proton spectra for nylon 6 fibers hydrated in D_2O: (a) spun at 500 m/min; (b) spun at 5000 m/min; (c) spun at 500 m/min and drawn at DR = 4.5. NMR spectra with broad and narrow components are detected.

IV. Results and Discussion

A. Proton NMR Spectra of Nylon 6 Fibers. Proton NMR spectra of nonrotating nylon 6 hydrated in D_2O are shown in Figure 7. The NMR spectra of the polymer can be decomposed into three components. One has the smallest full width at half-

TABLE 4: Relative Integral Intensities (A) and the Full-Width at Half Height ($\Delta\nu_{1/2}$) for Each Phase Obtained from a Decomposition of the Proton Spectra of Nylon 6 Fibers Hydrated in D_2O

	spun at 500 m/min			spun at 500 m/min DR = 4.5			spun at 5000 m/min		
	mobile amorp	less-mobile amorp	cryst	mobile amorp	less-mobile amorp	cryst	mobile amorp	less-mobile amorp	cryst
A[a] (%)	4.53	37.42	58.05	11.68	18.84	69.48	2.9	28.92	68.17
$\Delta\nu_{1/2}$[a] (kHz)	1.73	6.62	35.8	2.47	11.01	42.48	0.95	7.66	36.61

[a] The uncertainties are less than 10%.

TABLE 5: Proton Longitudinal Relaxation Times (T_1) and Relative Amplitudes (A) for Nonrotating Nylon 6 Fibers Hydrated in D_2O Derived from a Biexponential Fit[a]

	spun at 500 m/min	spun at 500 m/min DR = 4.5	spun at 5000 m/min
T_1^{long} (s)	1.67	2.53	1.82
T_1^{short} (s)	0.529	0.567	0.158
A^{long} (%)	93.8	87	97.8
A^{short} (%)	6.2	13	2.2

[a] The uncertainties are less than 10%.

height ($\Delta\nu_{1/2}$) in the range 0.95−2.47 kHz (see Table 4). It corresponds to the NMR mobile amorphous phase. From the integral intensity of the corresponding spectral component, it is evident that this phase has the smallest content. The nylon fiber spun at 5000 m/min shows a higher chain mobility accompanied by a reduction in the relative amount of this phase. The amount of mobile amorphous and crystalline phases is increased and the mobility of the polymer chains in the mobile amorphous chains is decreased by hot drawing of the nylon 6 fiber spun at a low winding speed of 500 m/min to a draw ratio of DR = 4.5 (cf. Table 4). The mobility of the polymer chains in the mobile amorphous phase is about 1 order of magnitude higher than that in the less-mobile amorphous phase. This allows a good selection of the z-magnetization of the former domain by use of a dipolar filter (see below). The data presented in Table 4 show that for all samples the content of the less-mobile amorphous and crystalline phases represents more than about 90%. Therefore, the spin-diffusion process with the mobile phase as the source of z-magnetization proceeds into a very large sink.

B. Relaxation of Longitudinal Proton Magnetization. The spin-diffusion process at long times is affected by relaxation of longitudinal magnetization. Therefore, to obtain spin-diffusion data to be described by the equation derived before, we performed a series of measurements of ^1H T_1 relaxation times of nylon 6 fibers hydrated in D_2O. The magnetization recovery can well be fitted with only two exponentials, and the values of long and short T_1 as well as the relative intensities of these components are shown in Table 5. The process of magnetization recovery under spin−lattice relaxation is affected by the spin-diffusion process. The fact that only two components can be detected shows that the process of spin-diffusion between less-mobile amorphous and crystalline phases is much faster compared to the longitudinal relaxation. Therefore, in agreement with the reported data for $T_{1\rho}$, the short values for T_1 are attributed to the mobile amorphous phase and the long values to the less-mobile amorphous and crystalline phases.[28] This assignment is also supported by the relative contributions of the integral amplitudes of the relaxation components. A contribution of 2.2%−13% is measured for the mobile amorphous phase. These values are in the same range as those reported before for the high-speed melt-spun nylon 6 fibers using $T_{1\rho}$ measurements.[28] A very small amount of mobile amorphous phase was detected for nylon fiber 6 fiber spun at 5000 m/min, and the highest value is obtained for the fiber spun at 500 m/min and drawn at DR = 4.5, in agreement with the data obtained from the decomposition of ^1H spectra (compare Tables 4 and 5).

TABLE 6: Proton Longitudinal Relaxation Times (T_1) and Relative Component Amplitudes (A) for Nylon 6 Fibers Hydrated in D_2O Measured under MAS at ν_R = 5 kHz[a]

	spun at 500 m/min	spun at 500 m/min DR = 4.5	spun at 5000 m/min
T_1^{long} (s)	1.091	1.99	1.55
T_1^{short} (s)	0.122	0.113	0.101
A^{long} (%)	91.88	89.64	97.9
A^{short} (%)	8.12	10.36	2.1

[a] The uncertainties are less than 10%.

To decouple the magnetization transfer from the mobile amorphous phase to the other two phases, we have decided to measure T_1 under partially fast MAS at ν_R = 5 kHz. The fast MAS condition is valid for the ^1H dipolar couplings of the mobile amorphous domains which exhibit a full width at half-height of the order of 1 kHz. The measurements of longitudinal relaxation in the laboratory reference frame were performed at the Larmor frequency ν_0 = 500 MHz. Because $\nu_0 \gg \nu_R$, a dependence of the longitudinal relaxation times on the rotor frequency is not expected. Furthermore, the reduction of the residual dipolar couplings will lead to slowing down of the spin-diffusion process in the mobile amorphous phase and as a consequence to an increase in the T_1 values. An opposite trend in the T_1 values was measured in our experiments (see Tables 5 and 6). This behavior was found[37] in a similar investigation made on model organic compounds such as adamantane and glycine and explained by the existence of dynamic heterogeneities resulting from, for instance, more mobile groups of the molecules or from different packing arrangements. Another possible explanation is the increase in the sample temperature in MAS experiments.[38] Because static as well as MAS measurements of longitudinal relaxation times are affected by the adverse effects, we used an average value, that is, $\bar{T}_1 = (T_{1,static} + T_{1,MAS})/2$ for the correction of the spin-diffusion data. Furthemore, from the results presented in Table 6 it is also evident that the values of the relative amounts of mobile amorphous and rigid amorphous/crystalline phases are just slightly different from the values obtained from T_1 data (see Table 5).

C. Dipolar Filter. To perform a spin-diffusion experiment, a gradient in the Zeeman spin order has to be created by using a chemical shift or a dipolar filter.[1] Two types of dipolar filters were employed in this study: (i) a Goldman−Shen dipolar filter[39] or a T_2 filter using the differences between the transverse magnetization decays of different domains and (ii) a MAPE filter (see Figure 1).[11] The latter one is based on the magic-, Hahn-, and polarization-echoes.[40−42] Compared to the T_2 filter, for which the efficiency in selecting the transverse magnetization is proportional to the ratio $T_{2,mobile}/T_{2,rigid}$, the MAPE filter has an efficiency in filtering out the single-quantum coherences of the rigid phase given by $(T_{2,mobile}/T_{2,rigid})^{6N}$, where N is the number of the magic sandwiches (cf. Figure 1).[11]

The efficiency of the T_2 and MAPE dipolar filters was measured for the nylon 6 fiber spun at 5000 m/min and hydrated in D_2O, and the results are shown in Figure 8. The Goldman−Shen filter with the pulse separation of 120 μs is quite efficient in filtering out the crystalline component (compare Figures 8a and b). Nevertheless, a small contribution from the rigid amorphous phase can be detected (cf. Figure 8b). A partial filtration is obtained when the MAPE filter is used with the

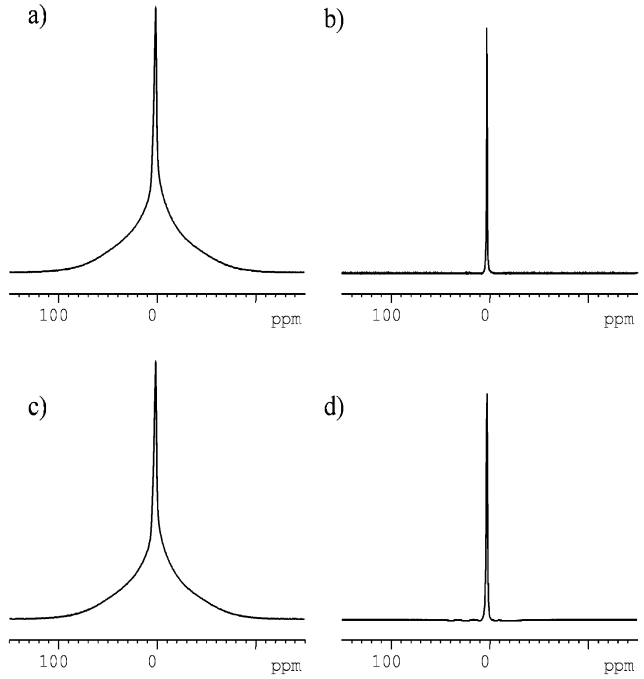

Figure 8. Dipolar filter efficiency for a nylon 6 fiber spun at 5000 m/min: (a) Proton spectrum obtained after Fourier transformation of the free induction decay recorded after a 90° radio frequency pulse. (b) Spectrum obtained using a Goldman−Shen filter[38] with a pulse separation of 120 μs. (c) Spectrum obtained using a MAPE filter[11] with the free evolution period of $\tau = 1$ μs and $N = 1$ (cf. Figure 1). (d) Spectrum after a MAPE filter with $\tau = 110$ μs and $N = 1$.

free evolution time of $\tau = 1$ μs and $N = 1$, as shown in Figure 8c. For $\tau = 110$ μs and $N = 1$, only the mobile amorphous component is present (cf. Figure 8d). The spectrum is not distorted (compare with Figure 8b), and its intensity is comparable to the intensity of the T_2 filtered ^{1}H spectrum. Therefore, the MAPE filter will be used for all the spin-diffusion experiments performed in this study.

D. Spin Diffusivities. The spin-diffusion coefficients characterizing the different domains first have to be evaluated before information on domain size and morphology can be inferred from the spin-diffusion data. We shall use two different methods for this purpose following the results presented in ref 11.

In the first method the spin-diffusion coefficient D can be evaluated by taking into account that, to a good approximation, the NMR line shape in the crystalline phase is Gaussian and is Lorentzian in less-mobile and mobile amorphous phases. The spin-diffusion coefficients can be related to the second van Vleck moment of the NMR absorption lines and to the full line width at half-height ($\Delta\nu_{1/2}$), that is,[11]

$$D_{\text{mobile}} \approx \frac{1}{6}\langle r^2\rangle[\alpha\Delta\nu_{1/2}]^2 \tag{13}$$

and

$$D_{\text{rigid}} \approx \frac{1}{12}\sqrt{\frac{\pi}{2\ln 2}}\langle r^2\rangle\Delta\nu_{1/2} \tag{14}$$

where $\langle r^2\rangle$ is the mean square distance between the nearest spins and α is a cutoff parameter for the Lorentzian line shape; that is, the absorption spectrum intensity is zero for the frequency range $|\Delta\omega| > \alpha$. To evaluate $\langle r^2\rangle$ for nylon 6, we have used a value of 0.18 nm for the distance between the protons of the methylene group and 0.25 nm for the nearest-neighbor protons in a CH_2-CH_2 molecular fragment.[43,44] Finally, the estimated weighted mean distance is $\langle r^2\rangle^{1/2} \approx 0.215$ nm. The values of the spin-diffusion coefficients for the three phases in nylon 6 fibers evaluated from this method are given in Table 7.

TABLE 7: Spin-Diffusion Coefficients (D) of Mobile Amorphous, Less-Mobile Amorphous, and Crystalline Domains for Nylon 6 Fibers Hydrated in D_2O[a]

	D (nm^2/ms)		
	mobile amorphous	less-mobile amorphous	crystalline
spun at 500 m/min	0.051[b]	0.198[b]	0.208[c] 0.244[d]
spun at 500 m/min; DR = 4.5	0.085[b]	0.225[b]	0.246[c] 0.289[d]
spun at 5000 m/min	0.034[b]	0.201[b]	0.213[c] 0.249[d]

[a] Using eq 13. [b] Using eq 14. [c] Using eq 15.

The second method for evaluating the diffusion coefficients is based on the experimentally measured spin-diffusion coefficient for a polymer with a well-defined morphology. The diffusivity for a symmetric diblock copolymer of poly(styrene) and poly(methyl metacrylate) (PS−PMMA) has been determined to be $D_{\text{PS-PMMA}} = (8 \pm 2)$ nm^2/ms.[5] The diffusivity for the crystalline domain can be evaluated using the scaling relation

$$D_{\text{crystalline}} = D_{\text{PS-PMMA}}\frac{\langle r^2\rangle_{\text{crystalline}}}{\langle r^2\rangle_{\text{PS-PMMA}}}\frac{[\Delta\nu_{1/2}]_{\text{crystalline}}}{[\Delta\nu_{1/2}]_{\text{PS-PMMA}}} \tag{15}$$

where $[\Delta\nu_{1/2}]_{\text{PS-PMMA}} \approx 76$ kHz and $\langle r\rangle^{1/2}_{\text{PS-PMMA}} \approx 0.25$ nm.[5] The values of the diffusivity for the crystalline domains in nylon 6 fibers obtained by this method are given in Table 7. The agreement between the values of $D_{\text{crystalline}}$ is reasonably good for the two methods.

E. Proton Spin-Diffusion on Nylon 6 Fibers. The spin-diffusion experiment using the pulse sequence shown in Figure 1 was applied to nylon 6 fibers hydrated in D_2O. The source of z-magnetization was selected by the MAPE dipolar filter in the mobile amorphous regions. The smaller number of protons in the mobile amorphous regions compared to that in the crystalline and less-mobile amorphous regions leads to broad signals with low integral intensity even at longer values of the spin-diffusion time (cf. Figure 9). Therefore, only the normalized intensities of the ^{1}H spectra corresponding to the mobile amorphous regions as a function of the square root of the diffusion time t are depicted in Figure 10.

The first method which is used for the evaluation of the size of the mobile amorphous domains is based on the intercept of the linear part of the spin-diffusion decay curve with the abscissa axis which yields the value $\sqrt{t_0^*}$ and which is related to the domain size by the relation[45]

$$d_{\text{mobile}} = \frac{2\epsilon}{\sqrt{\pi}}\sqrt{D_{\text{eff}}^* t_0^*} \tag{16}$$

where ϵ is the dimensionality of the spin-diffusion processes ($\epsilon = 1$ for lamellar morphology, $\epsilon = 2$ for cylindrical morphology, and $\epsilon = 3$ for spherical morphology) and

$$\sqrt{D_{\text{eff}}^*} = \frac{\sqrt{D_{\text{mobile}}D_{\text{eff}}}}{(\sqrt{D_{\text{mobile}}} + \sqrt{D_{\text{eff}}})/2}$$

where D_{eff} corresponds to the effective spin-diffusion coefficient of the sink. The sink corresponding to the B domains was considered to be represented by the crystalline and less-mobile

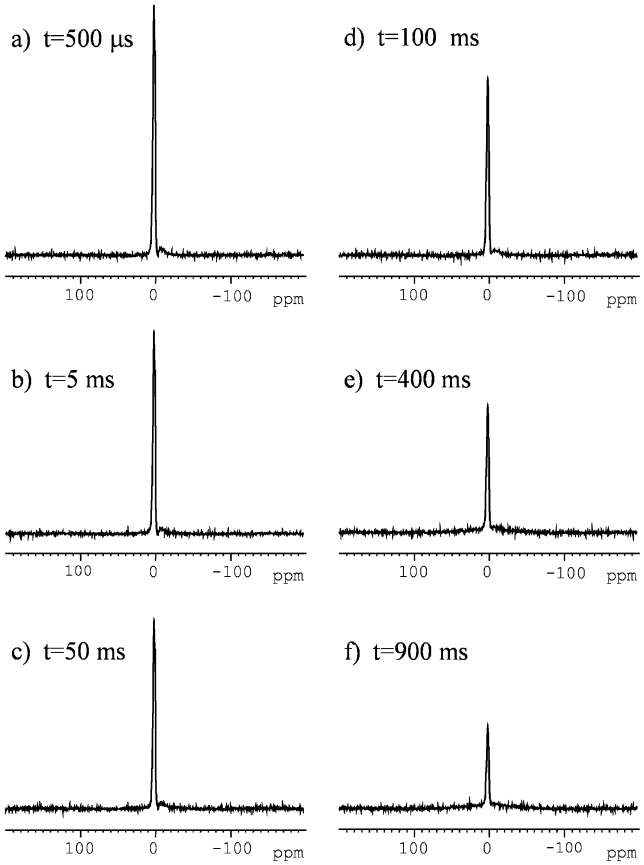

Figure 9. Proton NMR spectra recorded at different times t, for a spin-diffusion experiment (cf. Figure 1). A MAPE dipolar filter with $N = 1$ and $\tau = 110$ μs was used.

amorphous domains which have relatively close values of the diffusivities (cf. Table 7). These composite domains have an effective diffusivity given by

$$D_{\text{eff}} = \frac{N_{\text{c}}}{N} D_{\text{crystalline}} + \frac{N_{\text{lma}}}{N} D_{\text{less-mobile-amophous}} \qquad (17)$$

where the values of $D_{\text{less-mobile-amorphous}}$ and $D_{\text{crystalline}}$ were taken from Table 7. The corresponding relative fractions N_{c}/N and N_{lma}/N of the protons for the crystalline and less-mobile amorphous phases were taken from Table 8. It should be noted that the use of the parameter $\sqrt{t_0^*}$ instead of the parameter $\sqrt{t_{\text{m}}^{\text{s}}}$ used in ref 1 eliminates the dependence of d_{mobile} on the volume ratio of the sink to the source.[45] The estimated sizes of the mobile amorphous regions for the three nylon 6 samples based on a lamellar morphology and eq 16 are given in Table 9.

A more general method for evaluation of the domain sizes of all domains involved in the process of z-magnetization transfer is provided by use of eq 9, which is valid for a lamellar morphology and which describes the time evolution of the Zeeman polarization in the magnetization source in the limit of an ideal filter. The solid lines in Figure 10 are obtained from eq 9 using the diffusivities given in Table 7. For the sink we have used the same effective diffusion coefficient as that for the previous estimation. For the interface, the corresponding spin-diffusion coefficient has been taken to be an arithmetic average between the diffusivity of the composite domain and the diffusion coefficient of the mobile amorphous phase. The value of the proton density has been obtained on the basis of the molecular weight of the nylon 6 and of the densities of the

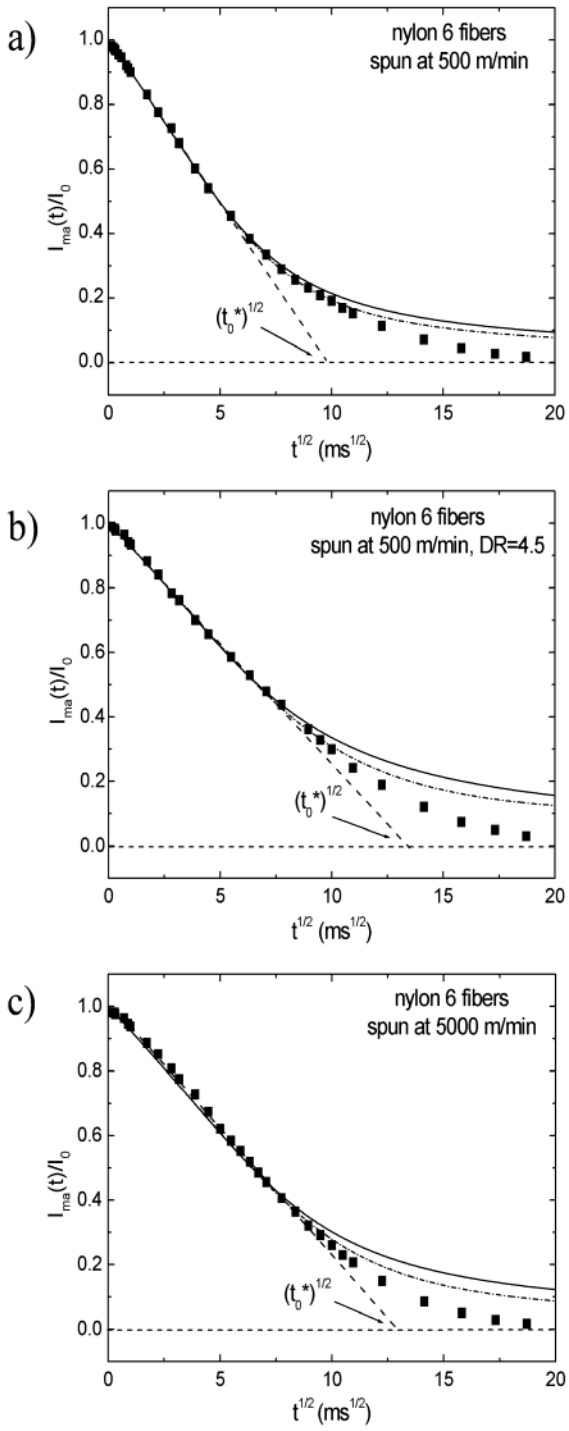

Figure 10. Normalized spin-diffusion decay curves for nylon 6 fibers (a) spun at 500 m/min without drawing, (b) drawn at DR = 4.5, and (c) spun at 5000 m/min obtained in a spin-diffusion experiment using a MAPE dipolar filter (see Figure 1). The intercept of the linear part of the decay curve with the time axis provides $(t_0^*)^{1/2}$. The best fits of the data using eq 9 and the diffusivities given in Table 7 are shown by solid lines. By the dash−dotted line shows the best fit when a value of 0.8 nm^2/ms is used for the diffusivity of the crystalline phase.

amorphous and crystalline phases, $\rho_{\text{amorphous}} = 1.09$ g/cm^3 and $\rho_{\text{crystalline}} = 1.18$ g/cm^3, respectively.[46] We have estimated a value of 0.105 g/cm^3 for the proton density of the amorphous phase and 0.108 g/cm^3 for the crystalline phase. An average value was used for the composite domain analogous to the value estimated for the spin-diffusion coefficient. Moreover, an average value from the proton density of the composite domain

TABLE 8: Relative Proton Fractions of Crystalline and Less-Mobile Amorphous Domains to the Mobile Amorphous Domains along the Fiber in Nylon 6 Fibers Hydrated in D_2O, Using the Relative Integral Intensities Reported in Table 4

	spun at 500 m/min	spun at 500 m/min; DR = 4.5	spun at 5000 m/min
$\{N_c\}/\{N\}$	0.6[a]	0.78[a]	0.70[a]
$\{N_{ra}\}/\{N\}$	0.39[a]	0.21[a]	0.29[a]

[a] The uncertainties are less than 10%.

TABLE 9: Domain Sizes (nm) of the Mobile Amorphous Phase, Interface, and Aggregate of Fibrils in the Nylon 6 Fibers in D_2O Obtained from an ^1H Spin-Diffusion Experiment, the Derived Analytical Solutions of the Spin-Diffusion Equations, and the Time Intercept $(t_0^*)^{1/2}$

	spun at 500 m/min	spun at 500 m/min; DR = 4.5	spun at 5000 m/min
mobile amorphous	3.69[a]	5.55[a]	3.79[a]
	3.46[b]	5.16[b]	3.64[b]
	3.8[c]	6.20[c]	4.20[c]
interface		0.75[b,c]	0.5[b,c]
	0.25[b,c]		
aggregate of fibrils	48[b]	40[b]	72[b]
	60[c]	50[c]	82[c]

[a] Using eq 16. The uncertainties are of the order of 20%. [b] Using eq 9. The uncertainties are of the order of 20%. [c] Using eq 9 and a diffusion coefficient of 0.8 nm^2/ms for the crystalline phase.[5]

and that of the mobile amorphous phase was used for the proton density of the interface.

The best fit of the spin-diffusion data using the above parameters gives the domain sizes of the three-domain morphology presented in Table 9. From Figure 10 it is evident that the simulated curves do not fit the spin-diffusion data in the long time regime. This fact could be related to the uncertainties in the ^1H NMR line shape decomposition at low signal-to-noise ratio and to the errors induced by the correction of the longitudinal magnetization relaxation at longer spin-diffusion times. However, the domain sizes of the mobile amorphous region estimated using the two methods are close to each other and are varying in the same way with the processing conditions.

An additional fit of the experimental data was made supposing that the spin-diffusion coefficient of the crystalline phase is 0.8 nm^2/ms, as reported in ref 5. The fitted curves are shown in Figure 10 by dash−dotted lines and seem to be better than the previous ones, but still the experimental data are not fitted in the long time regime. The obtained values for the domain sizes are reported also in Table 9. They are bigger than in the case of the previous fit, but they are still in the same range of values. This is due to the fact than an average diffusion coefficient is used for characterizing the spin-diffusion process in the domains represented by aggregate of fibrils.

F. Morphology of the Nylon 6 Fibers. Our particular setup of the spin-diffusion experiment in which the source of magnetization is selected for the mobile amorphous domains allows us to explore only some aspects of the complex morphology of the nylon 6 fiber. The structural model which can explain the measured domain sizes presented in Table 9 is shown in Figure 11. The highly mobile amorphous phase is situated at the surface of an aggregate of fibrils and separated from this aggregate by an interface. The magnetization transfer is taking place in a direction along the diameter of the fibrils. Inside of the aggregate, the fibrils are separated by the less-mobile amorphous domains. The fibrils have a lamellar structure with alternating crystalline and less-mobile amorphous domains.[47] The degree of fibrillar and lamellar orientation is about the same as that of the crystalline orientation.[47] It was shown by small-angle X-ray scattering (SAXS) that the interfibrillar regions, unlike the interlamellar regions, which essentially consist of amorphous chain segments, may have microvoids in addition to amorphous chain segments.[47] The morphology is similar to that discussed by Taylor and Clark[48] and recently by Hu and Schmidt-Rohr[21] for ultradrawn ultrahigh molecular weight polyethylene fibers to explain their ^1H spin-diffusion experiments.

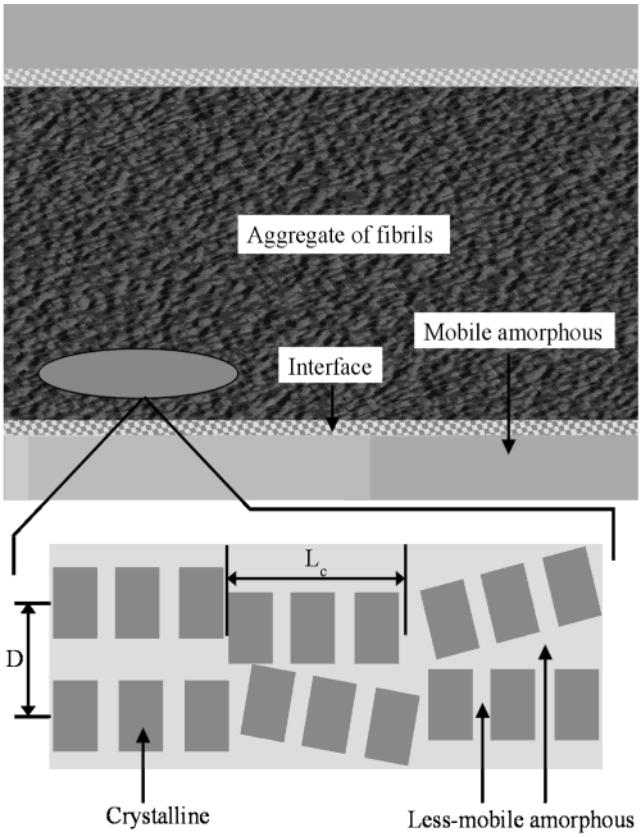

Figure 11. Model of the average phase morphology used for interpreting the spin-diffusion experiments with the source of the *z*-magnetization in the mobile amorphous phase. The number of protons in the mobile amorphous phase is in the range of about 2%−10% for investigated nylon 6 fibers hydrated in D_2O. The majority of protons are concentrated in the fibrils. The details not revealed by our spin-diffusion measurements about the aggregate of fibrils, but by SAXS, are also shown.[42] The distance between the fibrils is *D*. The fibrils are separated within the aggregate by the less-mobile amorphous domain. The axes of the fibrils are supposed to be oriented approximately parallel to the largest dimension of the interface and the mobile amorphous regions. Along the fibrils the lamellar stack of crystalline/less-mobile amorphous domains present is well organized within of a coherence length L_c.

The mobile amorphous phase has domain sizes in the range 3.4−6.2 nm for the investigated nylon 6 fibers. The process of hot drawing increases the size of these domains by a factor of about 2 and also the size of the interface compared to that of the fiber spun at 500 m/min (cf. Table 9). At the same time, the size of the aggregate of fibrils decreases compared to that when the fiber is not drawn. Not only are the domain sizes changing upon drawing but of course also the number of protons present in each domain is changing (cf. Table 4). For instance, the amount of mobile amorphous domains is increasing by about twice in the hot draw nylon 6 fiber compared to the undrawn fiber. This shows that the mobile amorphous phase formed in the process of hot drawing is mainly originating from the aggregation of fibrils and not from an extension of the polymer

chains in this phase. These results are supported by SAXS investigation of the drawing effect on nylon 6 fibers.[47] It was shown that the diameter of the fibrils decreases slightly upon drawing, in agreement with our reduced value of the size of the aggregation of fibrils (cf. Table 9). Moreover, the coherence length or the "crystallite size" begins to increase at the draw ratio 2.5−3.[47] This fact is supported by an increase of the relative number of protons detected by NMR in the crystalline phase of the drawn fiber (see Table 4). On the basis of the sizes given in Table 9 and the reported value of about 5 nm for the interfibril spacing of a nylon 6 fiber drawn to DR = 4.5,[47] the average number of fibrils present in the aggregates can be estimated to be in the range 4−8 using $D_{\text{crytalline}}$ values given in Table 7 and 7−10 for $D_{\text{crytalline}} = 0.8$ nm^2/ms.

The data presented in Table 9 show that for nylon 6 fibers spun at 5000 m/min the aggregate sizes increase by about 30% compared to the fibers spun at 500 m/min. This is in agreement with the larger value of the number of protons shown in Table 4. Also the domain sizes of the mobile amorphous phase and interface are increasing. The results from the ^{1}H line shape decomposition show that the less-mobile amorphous and mobile amorphous phases transform into the crystalline phase during high-speed spinning of the nylon 6 fibers (compare the *A* values for samples spun at 500 m/min and at 5000 m/min in Table 4). The same result was reported by Kwak et al.[28] for high-speed melt-spun nylon 6 fibers using various physical methods including solid-state ^{1}H NMR spectroscopy and relaxometry.

V. Conclusions

General analytical solutions valid for all time and space ranges of the spin-diffusion equations are reported for an arbitrary three-domain system with a lamellar morphology. The diffusion coefficients are supposed to be different in all the domains, and suitable boundary and initial conditions were taken into account. Moreover, these solutions can offer an approximate description of the diffusion process in two- and three-dimensions. The time and space evolution of the integral signal intensities were obtained for a dipolar filter which is supposed to be ideal; that is, the magnetization is present initially in just one source domain. These solutions can easily be generalized for the case of nonideal dipolar filters and for a distribution of domain sizes. The derived analytical solutions can be used in parallel with numerical procedures for testing the accuracy of the domain sizes measured by a spin-diffusion experiment. Moreover, the effects of the interface sizes and approximations made in estimating spin-diffusion coefficients can better be understood. Furthermore, these results represent the basis for obtaining analytical solutions for cylindrical and spherical morphologies.

Two different tests of domain sizes which can be obtained from the fit of spin-diffusion data with the analytical solutions were performed for a diblock copolymer and a semicrystalline polymer in which mainly a *z*-magnetization transfer in one-dimension takes place. Even if the domain sizes differ slightly from the values reported previously, they are in the same range of values. Thus, the derived equations represent a reliable tool for interpreting spin-diffusion measurements.

The complex morphology of nylon 6 fibers was tested using a dipolar filter which selects the *z*-magnetization of the NMR mobile amorphous domains. Complications arrising from the water of hydration were avoided by using fibers hydrated in D_2O. The experimental spin-diffusion data are interpreted in terms of a model in which *z*-magnetization transfer takes place into a series of parallel sinks of crystalline and less-mobile amorphous domains which form aggregates. The decay of the source *z*-magnetization is a monotonic function of time without plateaus which can be due to the flow of Zeeman order from alternating of crystalline and less-mobile amorphous domains with close values of diffusivities. These crystalline/less-mobile amorphous aggregates separated by mobile amorphous domains and probed by the spin-diffusion process involve about 4−10 fibrils. Probably a more realistic morphology involves a two-dimensional mobile amorphous phase surrounding the crystalline and less-mobile amorphous aggregates. If more dimensions are relevant for the magnetization transfer, for example, two for cylindrical domains, the smallest domain size found from the initial slope in the spin-diffusion plot increases in proportion with this dimensionality. Therefore, all the domain sizes reported in Table 9 have to be multiplied by $\epsilon = 2$, with large errors to account for the uncertainties in the shape and diffusivities of the domains.

The dipolar filters used in the spin-diffusion experiment can be set to provide the source of *z*-magnetization in the crystalline or in the mobile and less-mobile amorphous domains. Hence, this NMR experiment can probe some other aspects of the nylon 6 fiber morphology. The correlation between the changes in the domain sizes measured by these spin-diffusion experiments for a series of nylon 6 samples and the different draw ratios and spinning speeds can be exploited in order to establish processing−structure relationships. Work along these lines is in progress.

Appendix

To obtain analytical solutions for the spin-diffusion equations (eqs 1) with the initial and boundary conditions given by eqs 2−8, we introduce the Laplace transformation of the concentration of the *z*-magnetization $m_i(x,t)$, where i = A, B, and I, defined as

$$\bar{m}_i = \int_0^\infty e^{-pt} m_i(x,t)\, dt \tag{A1}$$

where p is a number whose real part is positive and large enough to make the above integral convergent. After the application of the Laplace transformation and taking into account that initially the magnetization is distributed only in domain A, we have to solve the following linear differential equations

$$\frac{\partial^2 \bar{m}_A}{\partial x^2} - q_A^2 \frac{\partial \bar{m}_A}{\partial t} = -\frac{m_0}{D_A}$$

$$\frac{\partial^2 \bar{m}_I}{\partial x^2} - q_I^2 \frac{\partial \bar{m}_I}{\partial t} = 0$$

$$\frac{\partial^2 \bar{m}_B}{\partial x^2} - q_B^2 \frac{\partial \bar{m}_B}{\partial t} = 0 \tag{A2}$$

where $q_A^2 = p/D_A$, $q_I^2 = p/D_I$, and $q_B^2 = p/D_B$.

Application of the Laplace transformation to the continuity conditions, eqs 4 and 5, yields

$$\bar{m}_A(l_1,t) = \bar{m}_I(l_1,t)$$

$$\bar{m}_I(l_2,t) = \bar{m}_B(l_2,t) \tag{A3}$$

and to the flux equalities (cf. eqs 6 and 7), yields

$$\rho_A D_A \frac{\partial \bar{m}_A(l_1,t)}{\partial x} = \rho_I D_I \frac{\partial \bar{m}_I(l_1,t)}{\partial x}$$

$$\rho_I D_I \frac{\partial \bar{m}_I(l_2,t)}{\partial x} = \rho_B D_B \frac{\partial \bar{m}_B(l_2,t)}{\partial x} \quad \text{(A4)}$$

The boundary conditions, eq 8, have the form

$$\frac{\partial \bar{m}_A(x,t)}{\partial x}|_{x=0} = 0 \quad \text{and} \quad \frac{\partial \bar{m}_B(x,t)}{\partial x}|_{x=l_3} = 0 \quad \text{(A5)}$$

The first of the equations (eqs A2) is an inhomogeneous linear differential equation with a solution of the form

$$\bar{m}_A = A_1 e^{q_A x} + B_1 e^{-q_A x} + \frac{m_0}{D_A {q_A}^2} \quad \text{(A6)}$$

where the first two terms represent the solution of the homogeneous differential equation and the last term is a particular solution.

The other two equations (eqs A2) are homogeneous differential equations, and we search solutions of the following form

$$\bar{m}_I = A_I e^{q_I x} + B_I e^{-q_I x}$$

$$\bar{m}_B = A_2 e^{q_B x} + B_2 e^{-q_B x} \quad \text{(A7)}$$

Using the boundary conditions, eqs A5, and following some algebra, all the unknown coefficients can be evaluated so that we obtain the following expressions for the Laplace transformation of the concentration of the nuclear spin z-magnetization in all three domains

$$\bar{m}_A = \frac{m_0}{D_A {q_A}^2}\left[1 - 2\rho_I\sqrt{D_I}ch(q_A x)\left(\frac{(\rho_I\sqrt{D_I} + \rho_B\sqrt{D_B})sh[q_I(l_2 - l_1) + q_B(l_3 - l_2)]}{E} + \frac{(\rho_I\sqrt{D_I} - \rho_B\sqrt{D_B})sh[q_I(l_2 - l_1) - q_B(l_3 - l_2)]}{E}\right)\right] \quad \text{(A8)}$$

$$\bar{m}_I = \frac{m_0}{D_A {q_A}^2}\left\{ch[q_I(x - l_1)] - \left(\frac{(\rho_I\sqrt{D_I} + \rho_B\sqrt{D_B})sh[q_I(l_2 - l_1) + q_B(l_3 - l_2)]}{E} + \frac{(\rho_I\sqrt{D_I} - \rho_B\sqrt{D_B})sh[q_I(l_2 - l_1) - q_B(l_3 - l_2)]}{E}\right)[(\rho_I\sqrt{D_I} + \rho_A\sqrt{D_A})ch[q_A l_1 + q_I(x - l_1)] + (\rho_I\sqrt{D_I} - \rho_A\sqrt{D_A})ch[q_A l_1 - q_I(x - l_1)]]\right\} \quad \text{(A9)}$$

and

$$\bar{m}_B = \frac{4m_0\rho_I\rho_A\sqrt{D_I D_A}}{{q_A}^2 D_A}\frac{sh(q_A l_1)ch[q_B(x - l_1)]}{E} \quad \text{(A10)}$$

where the quantity E is given by

$$E = (\rho_I\sqrt{D_I} + \rho_B\sqrt{D_B})(\rho_I\sqrt{D_I} + \rho_A\sqrt{D_A})sh[q_A l_1 + q_I(l_2 - l_1) + q_B(l_3 - l_2)] + (\rho_I\sqrt{D_I} + \rho_B\sqrt{D_B})(\rho_I\sqrt{D_I} - \rho_A\sqrt{D_A})sh[-q_A l_1 + q_I(l_2 - l_1) + q_B(l_3 - l_2)] + (\rho_I\sqrt{D_I} - \rho_B\sqrt{D_B})(\rho_I\sqrt{D_I} + \rho_A\sqrt{D_A})sh[q_A l_1 + q_I(l_2 - l_1) - q_B(l_3 - l_2)] + (\rho_I\sqrt{D_I} - \rho_B\sqrt{D_B})(\rho_I\sqrt{D_I} - \rho_A\sqrt{D_A})sh[-q_A l_1 + q_I(l_2 - l_1) - q_B(l_3 - l_2)] \quad \text{(A11)}$$

The next step is to apply the inverse Laplace transformation to eqs A8−A10. Our integrands have simple poles at $p = 0$ and $p = -D_A\beta_m^2$, where $\pm\beta_m$ are the roots of the trigonometric equation

$$(\rho_I\sqrt{D_I} + \rho_B\sqrt{D_B})(\rho_I\sqrt{D_I} + \rho_A\sqrt{D_A})\sin\left[\beta\left(l_1 + (l_2 - l_1)\sqrt{\frac{D_A}{D_I}} + (l_3 - l_2)\sqrt{\frac{D_A}{D_B}}\right)\right] + (\rho_I\sqrt{D_I} + \rho_B\sqrt{D_B})(\rho_I\sqrt{D_I} - \rho_A\sqrt{D_A})\sin\left[\beta\left(-l_1 + (l_2 - l_1)\sqrt{\frac{D_A}{D_I}} + (l_3 - l_2)\sqrt{\frac{D_A}{D_B}}\right)\right] + (\rho_I\sqrt{D_I} - \rho_B\sqrt{D_B})(\rho_I\sqrt{D_I} + \rho_A\sqrt{D_A})\sin\left[\beta\left(l_1 + (l_2 - l_1)\sqrt{\frac{D_A}{D_I}} - (l_3 - l_2)\sqrt{\frac{D_A}{D_B}}\right)\right] + (\rho_I\sqrt{D_I} - \rho_B\sqrt{D_B})(\rho_I\sqrt{D_I} - \rho_A\sqrt{D_A})\sin\left[\beta\left(-l_1 + (l_2 - l_1)\sqrt{\frac{D_A}{D_I}} - (l_3 - l_2)\sqrt{\frac{D_A}{D_B}}\right)\right] = 0 \quad \text{(A12)}$$

The residue of integrands A8−A10 at $p = 0$ is

$$m_0\frac{\rho_I(l_2 - l_1) + \rho_B(l_3 - l_2)}{\rho_A l_1 + \rho_I(l_2 - l_1) + \rho_B(l_3 - l_2)} \quad \text{for} \quad \bar{m}_A$$

and

$$m_0\frac{\rho_A l_1}{\rho_A l_1 + \rho_I(l_2 - l_1) + \rho_B(l_3 - l_2)} \quad \text{for} \quad \bar{m}_B$$

In the case of $\bar{m}_I$ we observe that for the first term we can directly apply the inverse Laplace transformation so that we must find the residue at $p = 0$ only for the second part, whose value is given by

$$m_0\frac{\rho_I(l_2 - l_1) + \rho_B(l_3 - l_2)}{\rho_A l_1 + \rho_I(l_2 - l_1) + \rho_B(l_3 - l_2)}$$

To calculate the residues at $p = -D_A\beta_m^2$, we have to evaluate

$$\frac{d}{dp}(pE)|_{p=-D_A\beta_m^2} = p\frac{dE}{dp}|_{p=-D_A\beta_m^2} \quad \text{or} \quad p\frac{dE}{dp}|_{p=-D_A\beta_m^2} = \frac{i\beta}{2}F \quad \text{(A13)}$$

where

$$F = (\rho_I\sqrt{D_I} + \rho_B\sqrt{D_B})(\rho_I\sqrt{D_I} + \rho_A\sqrt{D_A})\left[l_1 + (l_2 - l_1)\sqrt{\frac{D_A}{D_I}} + (l_3 - l_2)\sqrt{\frac{D_A}{D_B}}\right]\cos\left[\beta\left(l_1 + (l_2 - l_1)\sqrt{\frac{D_A}{D_I}} + (l_3 - l_2)\sqrt{\frac{D_A}{D_B}}\right)\right] + (\rho_I\sqrt{D_I} + \rho_B\sqrt{D_B})(\rho_I\sqrt{D_I} - \rho_A\sqrt{D_A})\left[-l_1 + (l_2 - l_1)\sqrt{\frac{D_A}{D_I}} + (l_3 - l_2)\sqrt{\frac{D_A}{D_B}}\right]\cos\left[\beta\left(-l_1 + (l_2 - l_1)\sqrt{\frac{D_A}{D_I}} + (l_3 - l_2)\sqrt{\frac{D_A}{D_B}}\right)\right] + (\rho_I\sqrt{D_I} - \rho_B\sqrt{D_B})(\rho_I\sqrt{D_I} + \rho_A\sqrt{D_A})\left[l_1 + (l_2 - l_1)\sqrt{\frac{D_A}{D_I}} - (l_3 - l_2)\sqrt{\frac{D_A}{D_B}}\right]\cos\left[\beta\left(l_1 + (l_2 - l_1)\sqrt{\frac{D_A}{D_I}} - (l_3 - l_2)\sqrt{\frac{D_A}{D_B}}\right)\right] + (\rho_I\sqrt{D_I} - \rho_B\sqrt{D_B})(\rho_I\sqrt{D_I} - \rho_A\sqrt{D_A})\left[-l_1 + (l_2 - l_1)\sqrt{\frac{D_A}{D_I}} - (l_3 - l_2)\sqrt{\frac{D_A}{D_B}}\right]\cos\left[\beta\left(-l_1 + (l_2 - l_1)\sqrt{\frac{D_A}{D_I}} - (l_3 - l_2)\sqrt{\frac{D_A}{D_B}}\right)\right] \quad \text{(A14)}$$

Applying now the inverse Laplace transformation to eqs A8−A10, we get the time dependent *z*-magnetization concentration during the spin-diffusion process

$$m_A = \frac{m_0\rho_A l_1}{\rho_A l_1 + \rho_I(l_2 - l_1) + \rho_B(l_3 - l_2)} - \sum_{m=1}^{\infty}\frac{4m_0\rho_I\sqrt{D_I}e^{-D_A\beta_m^2 t}\cos(\beta_m x)}{\beta_m F}\left\{(\rho_I\sqrt{D_I} + \rho_B\sqrt{D_B})\sin\left[\beta_m\left((l_3 - l_2)\sqrt{\frac{D_A}{D_B}} + (l_2 - l_1)\sqrt{\frac{D_A}{D_I}}\right)\right] + (\rho_I\sqrt{D_I} - \rho_B\sqrt{D_B})\sin\left[\beta_m\left(-(l_3 - l_2)\sqrt{\frac{D_A}{D_B}} + (l_2 - l_1)\sqrt{\frac{D_A}{D_I}}\right)\right]\right\} \quad \text{(A15)}$$

$$m_I = \frac{m_0\rho_A l_1}{\rho_A l_1 + \rho_I(l_2 - l_1) + \rho_B(l_3 - l_2)} - \sum_{m=1}^{\infty}\frac{2m_0 e^{-D_A\beta_m^2 t}}{\beta_m F}\left\{(\rho_I\sqrt{D_I} + \rho_B\sqrt{D_B})\sin\left[\beta_m\left((l_3 - l_2)\sqrt{\frac{D_A}{D_B}} + (l_2 - l_1)\sqrt{\frac{D_A}{D_I}}\right)\right] + (\rho_I\sqrt{D_I} - \rho_B\sqrt{D_B})\sin\left[\beta_m\left(-(l_3 - l_2)\sqrt{\frac{D_A}{D_B}} + (l_2 - l_1)\sqrt{\frac{D_A}{D_I}}\right)\right]\right\}\left\{(\rho_I\sqrt{D_I} + \rho_A\sqrt{D_A})\cos\left[\beta_m\left(l_1 + (x - l_1)\sqrt{\frac{D_A}{D_I}}\right)\right] + (\rho_I\sqrt{D_I} - \rho_A\sqrt{D_A})\cos\left[\beta_m\left(l_1 - (x - l_1)\sqrt{\frac{D_A}{D_I}}\right)\right]\right\} \quad \text{(A16)}$$

and

$$m_B = \frac{m_0\rho_A l_1}{\rho_A l_1 + \rho_I(l_2 - l_1) + \rho_B(l_3 - l_2)} + \sum_{m=1}^{\infty}\frac{8C_0\rho_I\rho_A\sqrt{D_I D_A}e^{-D_A\beta_m^2 t}\sin(\beta_m l_1)}{\beta_m F}\cos\left[\beta_m(l_3 - x)\sqrt{\frac{D_A}{D_B}}\right] \quad \text{(A17)}$$

These quantities are used for the evaluation of the integral *z*-magnetization of each domain given by eqs 9−11. The above sums are made over all solutions β_m of the trigonometric equation (eq A14).

Acknowledgment. This work was supported by grants from the Bundesministerium für Bildung und Forschung and Deutsche Forschungsgemeinschaft.

References and Notes

(1) Schmidt-Rohr, K.; Spiess, H. W. *Multidimensional Solid-State NMR and Polymers*; Academic Press: London, 1994.
(2) Blümich, B. *NMR Imaging of Materials*; Clarendon Press: Oxford, 2000.
(3) Kimmich, R. *NMR: Tomography, Diffusiometry, Relaxometery*; Springer-Verlag: Berlin, Heidelberg, New York, 1997.
(4) Demco, D. E.; Blümich, B. *Concepts Magn. Reson.* **2000**, *12*, 188 and 269.
(5) Clauss, J.; Schmidt-Rohr, K.; Spiess, H. W. *Acta Polym.* **1993**, *44*, 1.
(6) McBrierty, V. J.; Parker, K. J. *Nuclear Magnetic Resonance in Soild Polymers*; Cambridge University Press: Cambridge, U.K., 1993.
(7) VanderHart, D. L.; Manley, R. S. J.; Barnes, J. D. *Macromolecules* **1994**, *27*, 2826.
(8) VanderHart, D. L. *Macromolecules* **1994**, *27*, 2837.
(9) VanderHart, D. L.; McFadden, G. B. *Solid State Nucl. Magn. Reson.* **1996**, *7*, 45.
(10) VanderHart, D. L.; Asano, A.; Gilman, J. W. *Chem. Mater.* **2001**, *13*, 3781.
(11) Demco, D. E.; Johansson, A.; Tegenfeldt, J. *Solid State Nucl. Magn. Reson.* **1995**, *4*, 13.
(12) Cheung, T. T. P.; Gernstein, B. C. *J. Appl. Phys.* **1981**, *52*, 5517.
(13) Havens, J. R.; VanderHart, D. L. *Macromolecules* **1995**, *18*, 1663.
(14) Idiyatullin, D. Sh.; Khozina, E. V.; Smirnov, V. S. *Solid State Nucl. Magn. Reson.* **1996**, *7*, 17.
(15) Assink, R. A. *Macromolecules* **1978**, *11*, 1233.
(16) Kimura, T.; Neki, K.; Tamura, N.; Horri, F.; Nakagama, M.; Odani, H. *Polymer* **1992**, *33*, 493.
(17) Eijkelenboom, A. P. A. M.; Maas, W. E. J. K.; Veeman, W. S.; Werumens Buning, G. H.; Vankan, J. M. J. *Macromolecules* **1992**, *25*, 4511.
(18) Kenwright, A. M.; Say, B. J. *Solid State Nucl. Magn. Reson.* **1996**, *7*, 85.
(19) Weigand, F.; Demco, D. E.; Blümich, B.; Spiess, H. W. *J. Magn. Reson. A* **1996**, *120*, 190.
(20) Wang, J. *J. Chem. Phys.* **1996**, *4*, 4850.
(21) Hu, W.-G.; Schmidt-Rohr, K. *Polymer* **2000**, *41*, 2979.
(22) Gabrielse, W.; Angad Gaur, H.; Feyen, F. C.; Veeman, W. S. *Macromolecules* **1994**, *27*, 5811.
(23) Ziabicki, A. *Fundamentals of Fiber Formation*; Wiley: London, 1976.
(24) Hirschinger, J.; Miura, H.; Gardner, K. H.; English, A. D. *Macromolecules* **1990**, *23*, 2153.
(25) Miura, H.; Hirschinger, J.; English, A. D. *Macromolecules* **1990**, *23*, 2169.
(26) Murthy, N. S.; Bray, R. G.; Correals, S. T.; Moore, R. A. F. *Polymer* **1993**, *36*, 3863.
(27) Murthy, N. S.; Minor, H.; Bednarczyk, C. *Macromolecules* **1993**, *26*, 1712.
(28) Kwak, S.-Y.; Kim, J. H.; Kim, S. Y.; Jeong, H. G.; Kwon, I. H. *J. Polym. Sci., Part B: Polym. Phys.* **2000**, *38*, 1285.
(29) Kwak, S.-Y.; Kim, J. H.; Lee, J.-C. *J. Polym. Sci., Part B: Polym. Phys.* **2001**, *39*, 993.
(30) Adriansens, P.; Storme, L.; Carleer, R.; D'Haen, J.; Gelan, J.; Litvinov, V. M.; Marissen, R.; Crevecoeur, J. *Macromolecules* **2002**, *35*, 135.
(31) Hutchison, J. L.; Murthy, N. S.; Samulski, E. T. *Macromolecules* **1996**, *29*, 5551.

(32) Murthy, N. S.; Stamm, M.; Sibilia, J. P.; Krimm, S. *Macromolecules* **1989**, *22*, 1261.
(33) Adriaensens, P.; Pollaris, A.; Carleer, R.; Vanderzande, D.; Gelan, J.; Litvinov, V. M.; Tijssen, J. *Polymer* **2001**, *42*, 7943.
(34) Crank, J. *The Mathematics of Diffusion*; Clarendon Press: Oxford, U.K., 1986.
(35) Carslaw, H. S.; Jaeger, J. C. *Conduction of Heat in Solids*; Clarendon Press: Oxford, U.K., 1986.
(36) Cai, W. Z.; Schmidt-Rohr, K.; Egger, N.; Gerharz, B.; Spiess, H. W. *Polymer* **1993**, *34*, 267.
(37) Gil, A. M.; Alberti, E. *Solid State Nucl. Magn. Reson.* **1998**, *11*, 203.
(38) Langer, B.; Schnell, I.; Spiess, H. W.; Grimmer, A.-R. *J. Magn. Reson.* **1999**, *138*, 182.
(39) Goldman, M.; Shen, L. *Phys. Rev.* **1966**, *144*, 321.
(40) Rhim, W.-K.; Pines, A.; Waugh, J. S. *Phys. Rev. B* **1971**, *3*, 684.
(41) Demco, D. E. *Phys. Lett. A* **1973**, *45*, 113.
(42) Zhang, S.; Meier, B. H.; Ernst, R. R. *Phys. Rev. Lett.* **1992**, *69*, 2149.
(43) Northolt, M. G. *Acta Crystallogr.* **1970**, *B26*, 240.
(44) Bodor, G.; Bednowitz, A. L.; Post, B. *Acta Crystallogr.* **1967**, *23*, 482.
(45) Mellinger, F.; Wilhelm, M.; Spiess, H. W. *Macromolecules* **1999**, *32*, 4686.
(46) Brandrup, J.; Immergut, E. H. *Polymer Handbook*, 3rd ed.; John Wiley & Sons: New York, 1989.
(47) Murthy, N. S.; Bednarczyk, C.; Moore, R. A. F.; Grubb, D. T. *J. Polym. Sci., Part B: Polym. Phys.* **1996**, *34*, 821.
(48) Taylor, W. N.; Clark, E. S. *Polym. Eng. Sci.* **1978**, *18*, 518.